Structural and biochemical characterization of the laminarinase Zg LamC GH16 from Zobellia galactanivorans suggests preferred recognition of branched laminarin

Article *in* Acta Crystallographica Section D Biological Crystallography · February 2015

DOI: 10.1107/S139900471402450X · Source: PubMed

8 authors, including:

Murielle Jam
Station Biologique de Roscoff
22 PUBLICATIONS **471** CITATIONS
SEE PROFILE

Laurent Legentil
Ecole Nationale Supérieure de Chimie de Re…
50 PUBLICATIONS **384** CITATIONS
SEE PROFILE

Vincent Ferrières
Ecole Nationale Supérieure de Chimie de Re…
120 PUBLICATIONS **1,258** CITATIONS
SEE PROFILE

Gurvan Michel
Station Biologique de Roscoff
110 PUBLICATIONS **3,010** CITATIONS
SEE PROFILE

Acta Crystallographica Section D
Biological Crystallography
ISSN 1399-0047

Structural and biochemical characterization of the laminarinase *Zg*LamC$_{GH16}$ from *Zobellia galactanivorans* suggests preferred recognition of branched laminarin

Aurore Labourel,[a,b]‡ Murielle Jam,[a,b]‡ Laurent Legentil,[c,d] Balla Sylla,[c,d] Jan-Hendrik Hehemann,[a,b] Vincent Ferrières,[c,d] Mirjam Czjzek[a,b] and Gurvan Michel[a,b]*

[a]Sorbonne Universités, UPMC Université Paris 06, UMR 8227, Integrative Biology of Marine Models, Station Biologique de Roscoff, CS 90074, 29688 Roscoff CEDEX, France, [b]CNRS, UMR 8227, Integrative Biology of Marine Models, Station Biologique de Roscoff, CS 90074, 29688 Roscoff CEDEX, France, [c]Ecole Nationale Supérieure de Chimie de Rennes, CNRS, UMR 6226, 11 Allée de Beaulieu, CS 50837, 35708 Rennes CEDEX 7, France, and [d]Université Européenne de Bretagne, France

‡ These authors contributed equally to this work.

Correspondence e-mail: gurvan@sb-roscoff.fr

Received 10 July 2014
Accepted 7 November 2014

PDB references:
*Zg*LamC$_{GH16-E142S}$, 4crq; complex with thio-β-1,3-glucan, 4cte

Laminarin is a β-1,3-D-glucan displaying occasional β-1,6 branches. This storage polysaccharide of brown algae constitutes an abundant source of carbon for marine bacteria such as *Zobellia galactanivorans*. This marine member of the Bacteroidetes possesses five putative β-1,3-glucanases [four belonging to glycosyl hydrolase family 16 (GH16) and one to GH64] with various modular architectures. Here, the characterization of the β-glucanase *Zg*LamC is reported. The catalytic GH16 module (*Zg*LamC$_{GH16}$) was produced in *Escherichia coli* and purified. This recombinant enzyme has a preferential specificity for laminarin but also a significant activity on mixed-linked glucan (MLG). The structure of an inactive mutant of *Zg*LamC$_{GH16}$ in complex with a thio-β-1,3-hexaglucan substrate unravelled a straight active-site cleft with three additional pockets flanking subsites −1, −2 and −3. These lateral pockets are occupied by a glycerol, an acetate ion and a chloride ion, respectively. The presence of these molecules in the vicinity of the O6 hydroxyl group of each glucose moiety suggests that *Zg*LamC$_{GH16}$ accommodates branched laminarins as substrates. Altogether, *Zg*LamC is a secreted laminarinase that is likely to be involved in the initial step of degradation of branched laminarin, while the previously characterized *Zg*LamA efficiently degrades unbranched laminarin and oligo-laminarins.

1. Introduction

Found on rocky seashores in cold and temperate regions, brown seaweeds represent an estimated 70% of the primary biomass in these coastal areas (Duarte *et al.*, 2005). This abundant resource mainly consists of polysaccharides, either constituting cell walls (*e.g.* alginate, cellulose and sulfated fucoidans; Michel *et al.*, 2010*b*; Popper *et al.*, 2011) or carbon storage (laminarin; Michel *et al.*, 2010*a*). Laminarin represents up to 35% of the algal dry weight (O'Sullivan *et al.*, 2010). This small vacuolar β-1,3-D-glucan contains 25 linearly linked glucosyl residues on average and occasional β-1,6-linked branches (Percival & Ross, 1951). It is composed of two series: the minor G-series, which contains only glucose residues, and the more abundant M-series, which displays a D-mannitol residue at the reducing end (Read *et al.*, 1996). The presence of mannitol in laminarin is owing to a major horizontal gene-transfer event between the common ancestor of brown algae and an actinobacterium, which resulted in the acquisition of the bacterial biosynthetic pathway for mannitol (Michel *et al.*, 2010*a*; Rousvoal *et al.*, 2011; Groisillier *et al.*, 2014) and alginate (Michel *et al.*, 2010*b*). Moreover, an insoluble laminarin fraction has been characterized in some species such as *Laminaria hyperborea* and *Saccharina longicruris*. In both cases, these insoluble β-1,3-glucans are essentially unbranched (Nelson & Lewis, 1974; Rioux *et al.*, 2010).

Altogether, the different forms of laminarin constitute an abundant carbon source for seaweed-associated bacteria and other heterotrophic microbes living in coastal waters. However, knowledge of the degradation mechanisms of genuine laminarin by the relevant marine bacteria remains limited. Several β-1,3-glucanases from bacteria and fungi have been studied, but these organisms essentially originate from terrestrial environments (http://www.cazy.org; Lombard *et al.*, 2014) and degrade other types of β-1,3-glucans such as the fibrillar callose of plants or the insoluble β-1,3–1,6-glucans of fungal cell walls (Stone, 2009). Among the exceptions, the β-glucanase from *Rhodothermus marinus*, which belongs to family 16 of glycoside hydrolases (GH16), has been well studied (Krah *et al.*, 1998; Bleicher *et al.*, 2011), but this marine bacterium was isolated from an oceanic hot spring and this biotope does not contain algal laminarin. In contrast, *Zobellia galactanivorans* is a model bacterium for the bioconversion of algal polysaccharides. This flavobacterium was isolated from the red alga *Delesseria sanguinea* in Roscoff, Brittany (Barbeyron *et al.*, 2001) and has mostly been studied for the degradation of sulfated galactans from red seaweeds (agars, carrageenans and porphyrans; for reviews, see Michel & Czjzek, 2013; Martin *et al.*, 2014). Nonetheless, *Z. galactanivorans* can also assimilate polysaccharides from brown algae, such as alginate (Thomas *et al.*, 2012, 2013). After alginate, laminarin is the second most abundant polysaccharide from brown algae and this storage compound can be also used as a sole carbon source by *Z. galactanivorans*. Its genome contains five putative laminarinases: four from family 16 of glycoside hydrolases (GH16; *Zg*LamA–*Zg*LamD) and one from the GH64 family (*Zg*LamE). While to date the GH64 family contains only β-1,3-glucanases (Lombard *et al.*, 2014), the GH16 family is a large polyspecific family with at least 11 different known EC numbers. Interestingly, the GH16 family includes several enzymes specific for algal polysaccharides: κ-carrageenases (Michel *et al.*, 2001), β-agarases (Jam *et al.*, 2005), β-porphyranases (Hehemann *et al.*, 2010) and of course laminarinases. Based on phylogenetic and structural evidence, laminarinase has been proposed to be the ancestral activity in the GH16 family (Barbeyron *et al.*, 1998; Michel *et al.*, 2001), consistent with the ancient nature of β-1,3-glucans as storage polysaccharides in eukaryotes (Michel *et al.*, 2010*a*). The catalytic residues of the GH16 enzymes are the two glutamate residues found in the conserved signature E*X*D*X*(*X*)E. The first glutamate acts as a nucleophile, while the second glutamate is the acid/base catalyst (Keitel *et al.*, 1993; Juncosa *et al.*, 1994). The putative laminarinases from *Z. galactanivorans* possess various additional modules, such as carbohydrate-binding modules (*e.g.* CBM6 and CBM42) and PKD domains. The complexity of this enzymatic system suggests that each enzyme may have a different biological function. We have recently reported the first characterization of an enzyme from this laminarinolytic system, *Zg*LamA$_{GH16}$ (Labourel *et al.*, 2014). To deepen our understanding of the complementary functions of the β-glucanases from *Z. galactanivorans*, we have undertaken extensive characterization of the GH16 catalytic module of *Zg*LamC. Notably, the structure of an inactive mutant of *Zg*LamC$_{GH16}$ was determined in complex with a thio-β-1,3-glucan analogue.

2. Materials and methods

Except where mentioned otherwise, all chemicals were purchased from Sigma. The thio-β-1,3-hexaglucan was synthesized according to a known procedure (Sylla, 2010).

2.1. Cloning and site-directed mutagenesis of *Zg*LamC$_{GH16}$

The gene encoding the putative laminarinase *Zg*LamC was cloned as described previously (Groisillier *et al.*, 2010). Briefly, primers were designed to amplify the coding region corresponding to the GH16 catalytic module of *Zg*LamC, referred to as *Zg*LamC$_{GH16}$ (forward primer, GGGGGG**GGATCC**CAAAGATTACAACTTGGTCTGGCAAG; reverse primer, CCCCCC**CAATTG**TTACTTTTGGTAGACCCTTACGTAATCT), by PCR from *Z. galactanivorans* genomic DNA. After digestion with the restriction enzymes *Bam*HI and *Mfe*I, the purified PCR product was ligated using T4 DNA ligase into the expression vector pFO4 pre-digested with *Bam*HI and *Eco*RI, resulting in a recombinant protein with an N-terminal hexahistidine tag (plasmid p*Zg*LamC$_{GH16}$). This plasmid was used to transform *Escherichia coli* DH5α strain for storage and *E. coli* C43(DE3) strain for protein expression. Site-directed mutagenesis was performed using the QuikChange II site-directed mutagenesis kit (Stratagene) and the plasmid p*Zg*LamC$_{GH16}$. The two putative catalytic residues Glu137 and Glu142 were replaced by either a serine or an alanine (mutant E137A, forward primer TGGCCTGCCTGCGGG**GCA**ATAGATATCATGGAG, reverse primer CTCCATGATATCTAT**TGC**CCCGCAGGCAGGCCA; mutant E137S, forward primer TGGCCTGCCTGCGGG**TCA**ATAGATATCATGGAG, reverse primer CTCCATGATATCTAT**TGA**CCCGCAGGCAGGCCA; mutant E142A, forward primer GAAATAGATATCATG**GCG**CGCATCAATAACGCT, reverse primer AGCGTTATTGATGCG**CGC**CATGATATCTATTTC; mutant E142S, forward primer GAAATAGATATCATG**TCG**CGCATCAATAACGCT, reverse primer AGCGTTATTGATGCG**CGA**CATGATATCTATTTC). Mutant plasmids were sequenced to confirm that the mutation occurred at the correct position. These variant plasmids were also used to transform *E. coli* DH5α strain for storage and *E. coli* C43(DE3) strain for protein expression.

2.2. Overexpression and purification of *Zg*LamC$_{GH16}$ and *Zg*LamC$_{GH16\text{-}E142S}$

The *E. coli* C43(DE3) strain containing the plasmid p*Zg*LamC$_{GH16}$ was used to inoculate 3 ml Luria–Bertani (LB) broth medium supplemented with 100 µg ml^{-1} ampicillin. This preculture was incubated overnight at 37°C and 1 ml was transferred to inoculate 1 l of the auto-inducible ZYP 5052 medium (Studier, 2005). The culture was incubated at 20°C and 180 rev min^{-1} until the stationary phase was reached and was then harvested by centrifugation at 3000*g* and 4°C for 35 min. The cell pellet was stored at −20°C. The cells were

resuspended in 20 ml buffer *A* (20 m*M* Tris–HCl pH 7.5, 200 m*M* NaCl, 30 m*M* imidazole). An anti-protease mixture (cOmplete EDTA-free, Roche) and 0.1 mg ml^{-1} DNase were added. The cells were disrupted in a French press. After centrifugation at 12 500*g* for 2 h at 4°C, the supernatant was loaded onto a 10 ml Chelating Sepharose Fast Flow column (GE Healthcare) previously charged with 100 m*M* $NiSO_4$ and equilibrated with buffer *A*. The column was washed with buffer *A* (110 ml) and the protein was eluted with a 60 ml linear gradient from buffer *A* to buffer *B* (20 m*M* Tris–HCl pH 7.5, 200 m*M* NaCl, 500 m*M* imidazole) at a flow rate of 1 ml min^{-1}. The different fractions (1 ml each) were analyzed by SDS–PAGE. The fractions corresponding to a single band at the expected size (26 kDa) were pooled (13 ml) and were concentrated by ultrafiltration on an Amicon membrane (10 kDa cutoff; 4 ml at 7.5 mg ml^{-1}). Two aliquots of 2 ml (7.5 mg ml^{-1}) were loaded onto a 120 ml Superdex 75 column previously equilibrated with buffer *C* (20 m*M* Tris–HCl pH 7.5, 200 m*M* NaCl). The protein was eluted using between 70 and 80 ml buffer *C* and the purity of the fractions was checked by SDS–PAGE. 24 fractions of 1 ml each were pooled and a concentration of 1.25 mg ml^{-1} was determined using a NanoDrop spectrophotometer. A calibration curve was also used to determine the oligomerization state of *Zg*LamC$_{GH16}$. The mutant protein *Zg*LamC$_{GH16\text{-}E142S}$ was produced using the same procedure, but the buffers were different: buffer *A*′, 50 m*M* HEPES pH 7.5, 150 m*M* NaCl, 30 m*M* imidazole; buffer *B*′, 50 m*M* HEPES pH 7.5, 150 m*M* NaCl, 500 m*M* imidazole; buffer *C*′, 50 m*M* HEPES pH 7.5, 100 m*M* NaCl. *Zg*LamC$_{GH16\text{-}E142S}$ was concentrated by ultrafiltration on an Amicon membrane (10 kDa cutoff) to 13.6 mg ml^{-1}. The protein was filtrated on an Ultrafree Durapore PVDF 0.1 µm membrane before crystallization screening.

2.3. Thermostability analysis

The thermostability of *Zg*LamC$_{GH16}$ was studied by dynamic light scattering (DLS). 50 µl of a solution of *Zg*LamC$_{GH16}$ at 7.5 mg ml^{-1} was filtrated on a 0.2 µm membrane. Using a Zetasizer Nano (Malvern), the protein solution was heated from 10 to 70°C in steps of 1°C over a total period of 12 h and the hydrodynamic gyration radius (R_g) was measured at each step. The denaturation temperature was determined as the point of sharp change in R_g.

2.4. Enzymatic activity assays on β-glucans

The hydrolytic activities of the purified *Zg*LamC$_{GH16}$ and *Zg*LamC$_{GH16\text{-}E142S}$ were measured by the ferricyanide reducing-sugar assay (Kidby & Davidson, 1973) on different β-glucans: laminarin from *L. digitata* [0.1%(*w*/*v*)], carboxymethyl cellulose (CMC), mixed-linked glucan (MLG) from barley, curdlan from *Alcaligenes faecalis* and paramylon from *Euglena gracilis* [all at 0.2%(*w*/*v*)]. Since laminarin is a small polysaccharide, this substrate was reduced prior to its usage as previously reported (Labourel *et al.*, 2014). Reduced laminarin was hydrolyzed by 10 n*M* purified enzyme in 1 ml buffer *C* at 40°C for 30 min. Aliquots of the reaction mixture (40 µl) were taken at T_0, 10 min and 30 min and were added to 200 µl 5× ferricyanide reagent. The samples were boiled at 95°C for 15 min and cooled to 20°C before absorbance measurements at 420 nm. All experiments were undertaken in triplicate. A calibration curve with 0–3.33 m*M* glucose (0, 0.278, 0.556, 1.11, 1.67, 2.22, 2.78 and 3.33 m*M*) was used to calculate the amount of released reducing ends as glucose reducing-end equivalents. The activity of *Zg*LamC$_{GH16}$ on MLG, CMC, curdlan and paramylon was similarly measured, except that the reactions were monitored for 15 h. Aliquots were taken at T_0, 10 min, 1 h and 15 h.

The pH optimum for laminarin hydrolysis was determined as follows: 0.1%(*w*/*v*) laminarin was hydrolyzed by 10 n*M* *Zg*LamC$_{GH16}$ in a 500 µl reaction mixture at 40°C for 10 min. Different buffers (at 100 m*M*) were tested at a pH varying from 3 to 9 in 0.5 pH-unit increments: phosphate–citrate (pH 3–6), MOPS (pH 6–7.5), Tris–HCl (pH 7.5–8.5) and glycine (pH 8.5–9). Released reducing ends were measured as described above, except that aliquots of the reaction mixture (40 µl) were taken every 2 min.

The kinetic parameters of *Zg*LamC$_{GH16}$ on reduced laminarin and MLG were determined using 10 n*M* enzyme in 500 µl reaction mixture at 40°C in 100 m*M* phosphate–citrate pH 5.0. The amount of released reducing ends was measured as above. For each substrate, five concentrations were used: 0.06, 0.12, 0.24, 0.48, 0.96 and 1.28%(*w*/*v*) for laminarin and 0.05, 0.1, 0.15, 0.2 and 0.25%(*w*/*v*) for MLG. Aliquots of the reaction mixture (40 µl) were taken every 2 min for 10 min for laminarin and every 5 min for 25 min for MLG. For each substrate, K_m and k_{cat} were determined from a Lineweaver–Burk plot.

2.5. Fluorophore-assisted carbohydrate electrophoresis (FACE) analysis

0.5%(*w*/*v*) laminarin was hydrolyzed using 100 n*M* *Zg*LamC$_{GH16}$ in a reaction mixture consisting of 500 µl phosphate–citrate buffer pH 5.0 at 20°C. The temperature of 20°C was chosen to slow down the reaction in order to be able to determine the mode of action of *Zg*LamC$_{GH16}$. An aliquot of 20 µl (100 µg oligosaccharides) was taken at 2 min, 10 min, 30 min and 1 h. The samples were boiled to inactivate the enzyme and then dried in vacuum (SpeedVac). The FACE experiment was undertaken as described previously (Jackson, 1990). Briefly, the oligosaccharides were mixed with 2 µl 0.15 *M* 8-aminonaphthalene-1,3,6-trisulfonic acid (ANTS) and 5 µl 1 *M* $NaBH_3CN$. The reaction mixtures were incubated at 37°C for at least 3 h and dried in vacuum (SpeedVac). The oligosaccharides were resuspended in 20 µl 25% glycerol and 10 µl (50 µg) was loaded onto a 36% acrylamide gel. The migration was undertaken at 200 V and 4°C with 1× migration buffer (192 m*M* glycine, 25 m*M* Tris pH 8.5). The experiment was repeated using 0.5%(*w*/*v*) MLG (from barley) and 100 n*M* *Zg*LamC$_{GH16}$. The reaction mixture was incubated at 37°C and an aliquot of 20 µl was taken at 1, 2, 3, 4, 5 and 30 min.

100 µg of different commercial linear β-1,3-D-glucans (from laminaritriose to laminarihexaose; Megazyme) were

Table 1
Data-collection and refinement statistics for the crystal structures of *Zg*LamC$_{E142S}$.

Values in parentheses are for the highest resolution shell.

	*Zg*LamC$_{GH16\text{-}E142S}$ 'apo form'	*Zg*LamC$_{GH16\text{-}E142S}$–thio-β-1,3-glucan
Data collection		
Beamline	PROXIMA1	BM-14
Wavelength	0.98	0.95
Space group	$P2_12_12_1$	$P2_12_12_1$
Unit cell-parameters (Å, °)	a = 67.11, b = 68.06, c = 143.28, $\alpha = \beta = \gamma$ = 90	a = 56.35, b = 94.01, c = 143.13, $\alpha = \beta = \gamma$ = 90
Resolution range (Å)	49.34–1.50 (1.58–1.50)	35.00–1.77 (1.87–1.77)
Total data	701835	637622
Unique data	105701	74817
Completeness (%)	99.80 (98.50)	100.00 (99.90)
Mean $I/\sigma(I)$	17.9 (2.60)	16.6 (3.30)
R_{merge}† (%)	5.0 (69.1)	7.8 (59.7)
$R_{p.i.m.}$‡ (%)	2.1 (29.0)	2.8 (22.2)
Multiplicity	6.6	8.5
Refinement statistics		
Resolution range	71.64–1.50 (1.54–1.50)	78.39–1.80 (1.85–1.80)
Unique reflections	100306 (6840)	66529 (4479)
Reflections for R_{free}	5274 (390)	3536 (241)
R/R_{free} (%)	15.0/18.6 (27.3/30.4)	17.9/22.2 (26.4/31.7)
R.m.s.d., bond lengths (Å)	0.016	0.020
R.m.s.d., bond angles (°)	1.68	1.98
B factor (Å^2)		
Overall	27.8	33.8
Molecule *A*	28.8	40.4
Molecule *B*	24.1	25.4
Solvent	40.0	43.0
Ligands§	32.4	*C*, 41.0; *D*, 34.5; *E*, 32.2; *F*, 30.1
No. of non-H atoms		
Protein	*A*, 1850; *B*, 1872	*A*, 1880; *B*, 1884
Ions	*A*, 3; *B*, 5	*A*, 2; *B*, 3
Ligand	*A*, 16; *B*, 12	*A*, 33; *B*, 48
Solvent	*A*, 191; *B*, 235	*A*, 142; *B*, 191
Ramachandran statistics (%)		
Most favoured	89.5	90.0
Additionally allowed	10.0	9.5
Disallowed	0.5	0.5
PDB entry	4crq	4cte

† $R_{merge} = \sum_{hkl}\sum_i |I_i(hkl) - \langle I(hkl)\rangle| / \sum_{hkl}\sum_i I_i(hkl)$, where the summation is over all symmetry-equivalent reflections. ‡ $R_{pim} = \sum_{hkl}\{1/[N(hkl)-1]\}^{1/2} \sum_i |I_i(hkl) - \langle I(hkl)\rangle| / \sum_{hkl}\sum_i I_i(hkl)$ and corresponds to the multiplicity-weighted R_{merge}. § *C*, inhibitor in chain *A*; *D*, inhibitor in chain *B*; *E*, glycerol in chain *A*; *F*, ethylene glycol in chain *B*.

hydrolyzed using 4.5 µ*M* *Zg*LamC$_{GH16}$ in a reaction mixture consisting of 100 µl phosphate–citrate buffer pH 5.0 at 37°C for 12 h. For each sample, an aliquot containing 50 µg oligosaccharides was treated as mentioned above. 5 µl (12.5 µg) were loaded onto a 36% acrylamide gel.

A glucan tetrasaccharide containing two β-1,4-linkages separated by one β-1,3-linkage (G4G3G4G) was also purchased from Megazyme. Three samples of this substrate at 50 µg were labelled with ANTS as described previously. One of them was used as a control. The second sample was resuspended in a 50 µl reaction mixture consisting of 4.5 µ*M* *Zg*LamC$_{GH16}$ and phosphate–citrate buffer pH 5.0 at 37°C for 30 min. The same experiment was undertaken on the third sample, except that *Zg*LamC$_{GH16}$ was first inactivated by heating. In parallel, 100 µg nonlabelled G4G3G4G was hydrolyzed by *Zg*LamC$_{GH16}$ at 37°C for 30 min. After the enzymatic reaction, an aliquot containing 50 µg oligosaccharides (reaction products) was labelled as mentioned above. A sample of 50 µg of glucose was also labelled with ANTS and was used as a control. 10 µl (25 µg) of each sample was loaded onto a 36% acrylamide gel.

2.6. Crystallization and structure refinement

Crystallization screening was undertaken with a Honeybee nanodrop robot (Cartesian) using the commercial screens The PACT and JCSG+ Suites (Qiagen). Using the sitting-drop vapour-diffusion method, 300 nl protein solution was mixed with 150 nl reservoir solution. The best initial crystallization condition was further optimized in 24-well Linbro plates by the hanging-drop vapour-diffusion method at 20°C. Single crystals of *Zg*LamC$_{GH16\text{-}E142S}$ were obtained by mixing 2 µl enzyme/oligosaccharide mixture with 1 µl reservoir solution and equilibrating against 750 µl reservoir solution. In the first case (corresponding to PDB entry 4crq), the 2 µl drop consisted of 8.6 mg ml^{-1} *Zg*LamC$_{GH16\text{-}E142S}$ and 1 m*M* purified laminaritetraoses produced by *Zg*LamA$_{GH16}$. The reservoir solution comprised 14% PEG 6000, 100 m*M* sodium acetate pH 5.0, 220 m*M* $MgCl_2$, 10% glycerol. In the second case (corresponding to PDB entry 4cte), the 2 µl drop consisted of 12.2 mg ml^{-1} *Zg*LamC$_{GH16\text{-}E142S}$ and 1 m*M* thio-β-1,3-hexaglucan substrate. This substrate was synthesized as described previously (Sylla, 2010). The reservoir solution consisted of 11% PEG 6000, 100 m*M* sodium acetate pH 5.0, 220 m*M* $MgCl_2$, 4% 2-propanol, 3% glycerol. Prior to flash-cooling in a nitrogen stream at 100 K, single crystals were quickly soaked in their reservoir solution supplemented with 30% ethylene glycol (for both types of crystals). Diffraction data for the crystals of *Zg*LamC$_{GH16\text{-}E142S}$ obtained in the presence of laminaritetraoses (hereafter referred to as the 'apo' form of *Zg*LamC$_{GH16\text{-}E142S}$; PDB entry 4crq) were collected on the PROXIMA1 beamline at the SOLEIL synchrotron, Saint-Aubin, France. The diffraction data for the *Zg*LamC$_{GH16\text{-}E142S}$–thio-β-1,3-hexaglucan complex (PDB entry 4cte) were collected on beamline BM14 at the ESRF synchrotron, Grenoble, France. X-ray diffraction data were integrated using *MOSFLM* (Leslie, 2006) and scaled with *SCALA* (Evans, 2006). The structure of *Zg*LamC$_{GH16\text{-}E142S}$ was determined by molecular replacement with *MOLREP* (Vagin & Teplyakov, 2010) using chain *A* of the laminarinase from *Thermotoga maritima* MSB8 (PDB entry 3azx; Jeng *et al.*, 2011) as a starting model. The structure of *Zg*LamC$_{GH16\text{-}E142S}$ was built using *Coot* (Emsley *et al.*, 2010) by modifying and completing this starting model. For the *Zg*LamC$_{GH16\text{-}E142S}$–inhibitor complex, the structure was also determined by molecular replacement but using the coordinates of chain *A* of *Zg*LamC$_{GH16\text{-}E142S}$ (the 'apo' form). For all of the structures, the initial molecular-replacement solutions were further refined with *REFMAC*5 (Vagin *et al.*, 2004) alternating with cycles of manual rebuilding using *Coot*. A subset consisting of a randomly selected 5% of the reflections was excluded from computational refinement to calculate the R_{free} factors

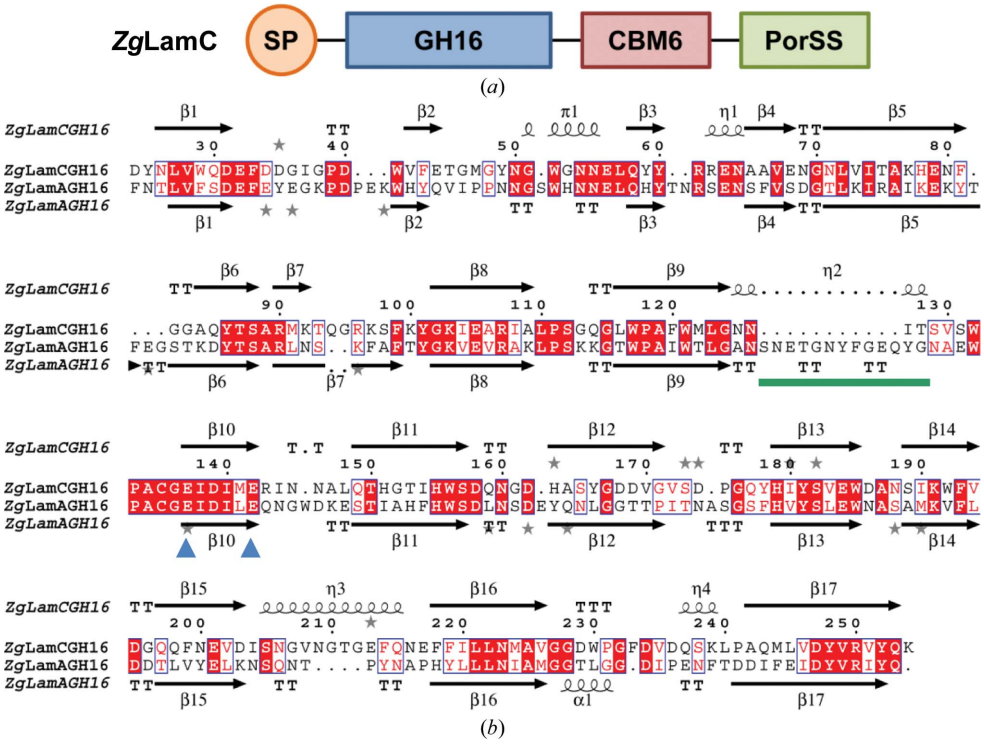

Figure 1
(*a*) Schematic representation of the β-glucanase *Zg*LamC from *Z. galactanivorans*. *Zg*LamC displays an N-terminal signal peptide (SP) followed by a catalytic module from the family 16 glycoside hydrolases (GH16), a family 6 carbohydrate-binding module (CBM6) and a C-terminal targeting domain specific to the *Porphyromonas*-like secretion system (PorSS). (*b*) Structure-based sequence alignment of *Zg*LamC$_{GH16}$ and *Zg*LamA$_{GH16}$ (PDB entry 4bow). α-Helices and β-strands are represented as helices and arrows, respectively, and β-turns are marked TT. Dark shaded boxes enclose invariant positions and light shaded boxes show positions with similar residues. The green bar corresponds to the additional loop in *Zg*LamA$_{GH16}$ that confers a bent active site to this laminarinase. The blue triangles indicate the catalytic glutamate residues that are conserved in all GH16 enzymes. This figure was created with *ESPript* (Gouet *et al.*, 2003).

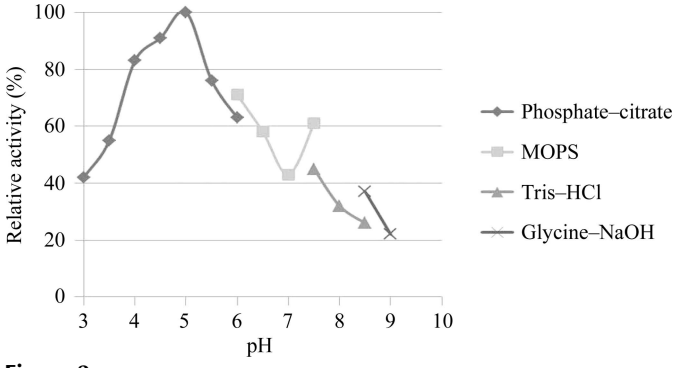

Figure 2
Effect of the pH on the activity of *Zg*LamC$_{GH16}$. The experiments were undertaken at 40°C in 100 m*M* buffer with 10 n*M* purified enzyme and 0.1%(*w*/*v*) laminarin. The activity in phosphate–citrate pH 5.0 buffer was considered as a reference for the maximum activity.

throughout refinement. The addition of the ligand sugar units for the complex structure was performed manually using *Coot*. Water molecules were added automatically with *REFMAC–ARP*/*wARP* and were visually verified. The final refinement was carried out using *REFMAC* with TLS, isotropic *B* factors, automatic NCS restraints and Babinet solvent scaling for the two *Zg*LamC$_{GH16\text{-}E142S}$ structures. Data-collection and refinement parameters are presented in Table 1.

3. Results

3.1. *Zg*LamC$_{GH16}$ is a monomeric β-glucanase active on laminarin and MLG

The putative laminarinase *Zg*LamC (GenBank CAZ95067) features an N-terminal cleavable signal peptide followed by a catalytic module of family 16 of the glycoside hydrolases (GH16), a central carbohydrate-binding module of family 6 (CBM6) and a C-terminal PorSS module (Fig. 1*a*). The Por secretion system (PorSS) is a recently described protein-secretion machinery that is unique to the Bacteroidetes phylum (Sato *et al.*, 2010), and the PorSS modules are conserved C-terminal domains that are likely to be involved in the targeting of proteins to the PorSS (Karlsson *et al.*, 2004; McBride & Zhu, 2013). The GH16 catalytic module of ZgLamC has 37% sequence identity to the homologous domain of *Zg*LamA (Fig. 1*b*), which we have recently characterized (Labourel *et al.*, 2014). The nucleotide sequence of this module was cloned in the pFO4 vector and expressed in *E. coli* C43(DE3) cells as a soluble protein referred to as *Zg*LamC$_{GH16}$. Two purification steps [immobilized metal-affinity chromatography (IMAC) and size-exclusion chromatography (SEC)] were needed to purify this recombinant protein and we obtained 30 mg pure protein per litre of culture. This sample was divided into two aliquots: the first for biochemical characterization (1 ml at 1.25 mg ml^{-1}) and the second for crystallization assays (23 ml at 1.25 mg ml^{-1}). The SEC experiment and DLS analysis indicate that *Zg*LamC$_{GH16}$ is a monomer in solution. DLS was also used to study the thermostability of the protein. A sharp increase in R_g was observed above 40°C, corresponding to the beginning of protein denaturation. The enzyme activity was tested by the ferricyanide reducing-sugar assay (Kidby & Davidson, 1973) on various β-glucans: soluble laminarin, MLG and CMC, and crystalline curdlan and paramylon. Activity was only detected in the presence of laminarin and MLG. *Zg*LamC$_{GH16}$ is active over a wide range of pH (from 3 to 9) and its optimal activity is observed in 100 m*M* phosphate citrate pH 5.0 (Fig. 2). Although the inhibitory effect of Tris–HCl on *Zg*LamC$_{GH16}$ is less drastic than that on *Zg*LamA$_{GH16}$

(Labourel *et al.*, 2014), an inhibitory effect is observed for this buffer at pH 7.5 (and to a lesser degree with phosphate–citrate buffer pH 6.0) in comparison to MOPS buffer (Fig. 2). This inhibitory effect of Tris–HCl buffer has been reviewed previously (Roberts & Davies, 2012). The activity of *Zg*LamA$_{GH16}$ was also assayed by a reducing-sugar assay at different temperatures, and 40°C was determined to be the optimal temperature for kinetic characterization (data not shown). The kinetic parameters of *Zg*LamC$_{GH16}$ were thus determined at 40°C and in phosphate–citrate buffer pH 5.0 on reduced laminarin and on MLG. While the Michaelis constant for laminarin is better than that for MLG (K_m of 4.83 ± 0.43 and 36.7 ± 4.2 m*M*, respectively), the turnover of *Zg*LamC$_{GH16}$ is surprisingly lower for laminarin than for MLG (k_{cat} of 286 ± 14 and 795 ± 134 s^{-1}, respectively). Nonetheless, the catalytic efficiency of *Zg*LamC$_{GH16}$ remains three times higher for laminarin than for MLG (k_{cat}/K_m of 59 213 and 21 662 M^{-1} s^{-1}, respectively).

Based on the knowledge of the catalytic residues in GH16 lichenases (Keitel *et al.*, 1993; Juncosa *et al.*, 1994) and on sequence comparison, one can predict that Glu137 and Glu142 are the nucleophile and acid/base catalyst of *Zg*LamC$_{GH16}$

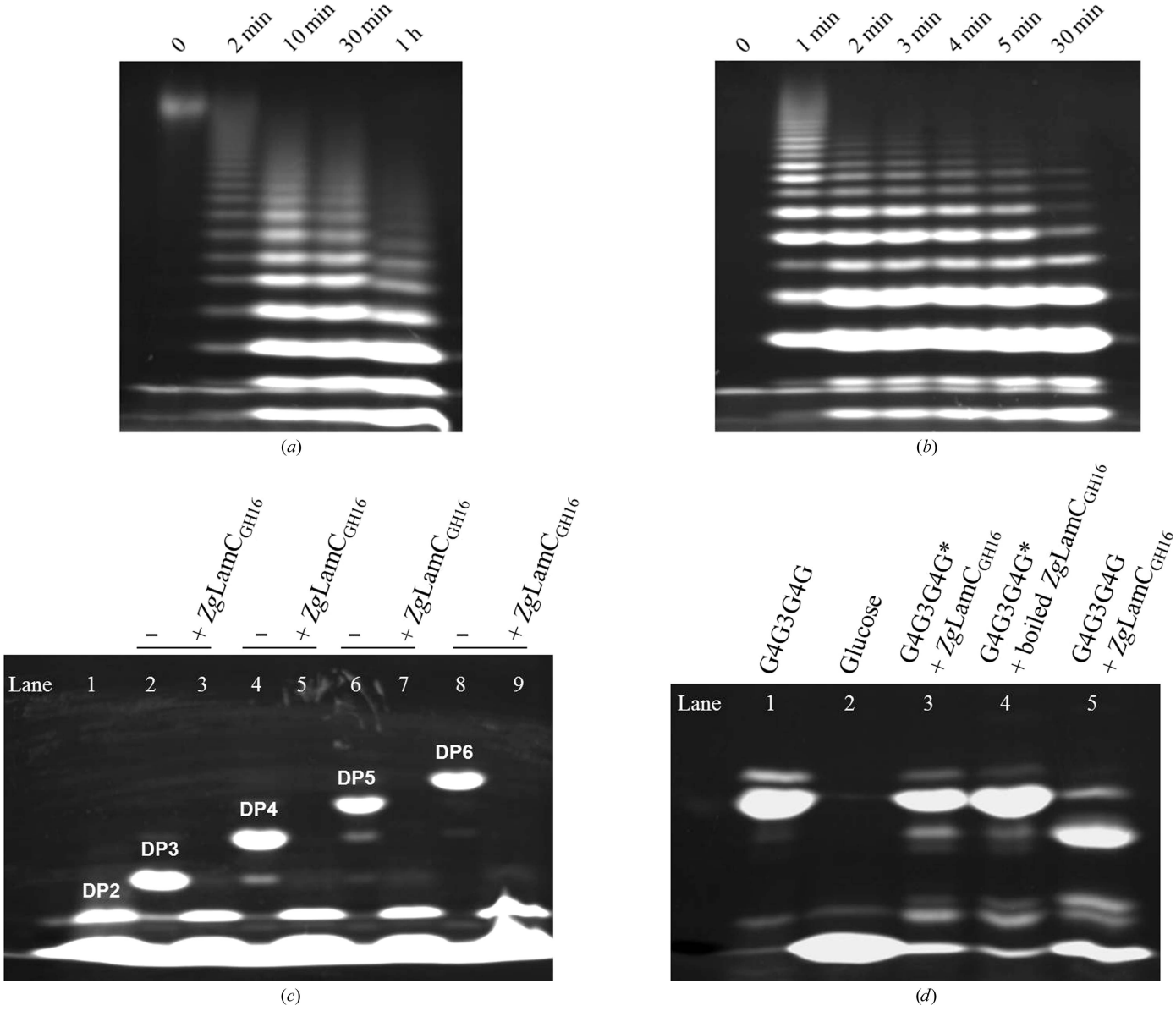

Figure 3
Mode of action and terminal products of *Zg*LamC$_{GH16}$. The hydrolysis of laminarin (*a*, *c*) and mixed-linked glucan (MLG) (*b*, *d*) by *Zg*LamC$_{GH16}$ was monitored by fluorophore-assisted carbohydrate electrophoresis (FACE). (*a*) 0.5%(*w*/*v*) laminarin was hydrolyzed by 100 n*M* *Zg*LamC$_{GH16}$ at 20°C. (*b*) 0.5%(*w*/*v*) MLG was hydrolyzed by 4.5 µ*M* *Zg*LamC$_{GH16}$ at 37°C. (*c*) Standard laminarin oligosaccharides are labelled from DP2 to DP6 (lanes 1, 2, 4, 6 and 8). 100 µg of the oligosaccharides from DP3 to DP6 at 0.1% were incubated with 4.5 µ*M* *Zg*LamC$_{GH16}$ at 37°C for 12 h (lanes 3, 5, 7 and 9). (*d*) The reaction mixtures contain 0.1%(*w*/*v*) of the tetrasaccharide G4G3G4G and 4.5 µ*M* active (lane 3 and 5) or inactive (lane 4) *Zg*LamC$_{GH16}$ in 100 m*M* phosphate–citrate pH 5.0 at 37°C for 30 min. An asterisk indicates that the G4G3G4G oligosaccharides were labelled before the enzymatic reaction, while the absence of an asterisk indicates that the oligosaccharides were labelled after the reaction.

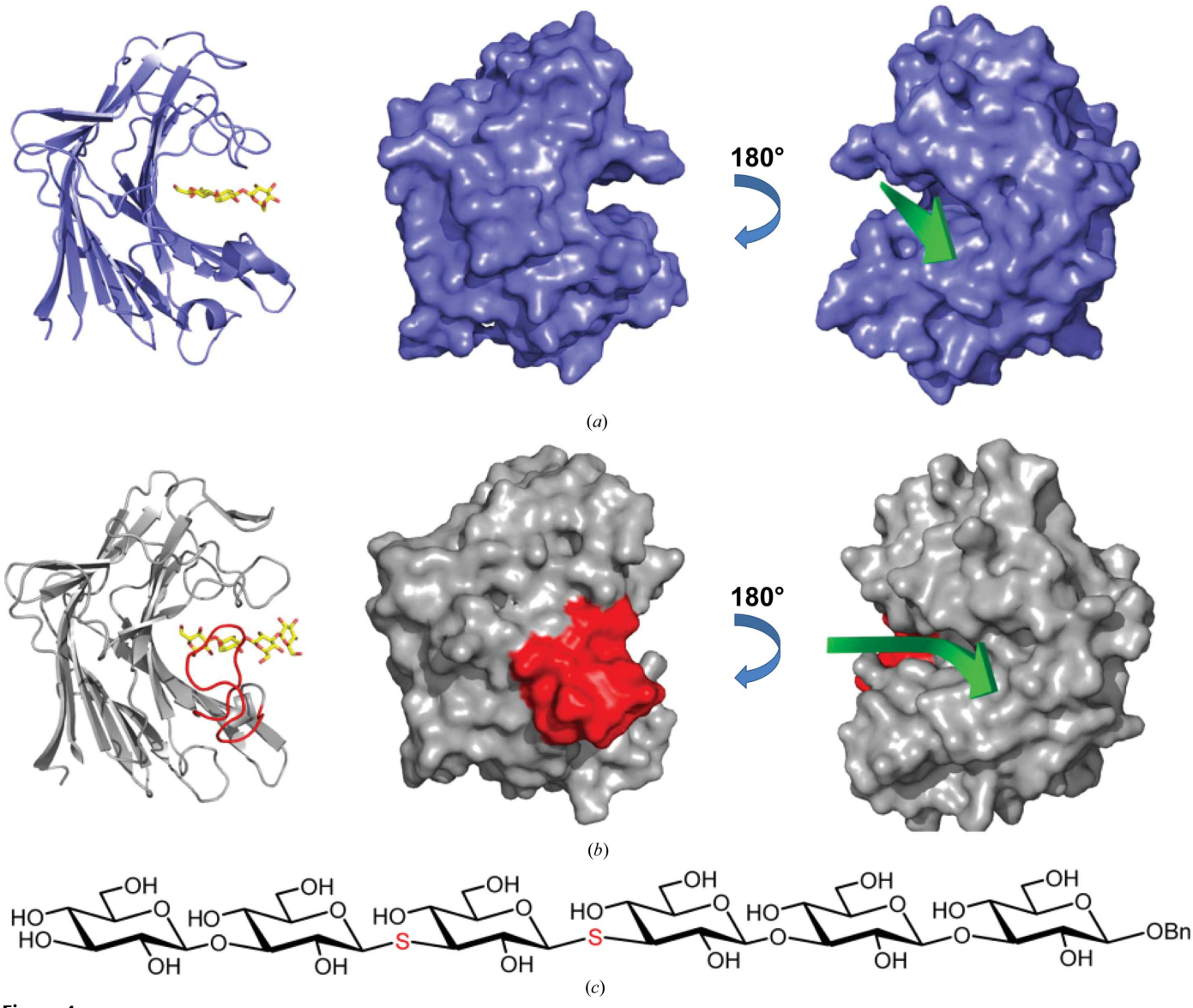

Figure 4
Comparison of the active-site topology of *Zg*LamC$_{GH16\text{-}E142S}$ and *Zg*LamA$_{GH16\text{-}E269S}$. (*a*) Cartoon representation of *Zg*LamC$_{GH16\text{-}E142S}$ in complex with the thio-β-1,3-glucan substrate. The substrate is shown in sticks. Surface representation of *Zg*LamC$_{GH16\text{-}E142S}$ with the same orientation as in the previous cartoon representation and after a 180° rotation. The green arrow highlights the straight topology of the active groove. (*b*) Cartoon representation of *Zg*LamA$_{GH16\text{-}E269S}$ in complex with laminaritetraose (PDB entry 4bow). The additional loop of *Zg*LamA$_{GH16\text{-}E269S}$ is coloured red. The substrate is shown in sticks. Surface representation of *Zg*LamA$_{GH16\text{-}E269S}$, with the same orientation as in the previous cartoon representation and after a 180° rotation. The surface corresponding to the additional loop is coloured red. The green arrow highlights the bent topology of the active groove. (*c*) Schematic representation of the thio-β-1,3-hexaglucan. (*a*) and (*b*) were made with *PyMOL*.

(Fig. 1), respectively. In order to obtain the structure of an inactive form of *Zg*LamC$_{GH16}$ in complex with laminarin or MLG oligosaccharides, we undertook the mutagenesis of these putative catalytic residues (E137A, E137S, E142A and E142S). Among these four site-directed mutations, only the replacement of the codon for Glu142 by a serine codon was confirmed by sequencing of the extracted plasmids. The protein corresponding to this mutated plasmid was expressed in soluble form in *E. coli* C43(DE3) cells and is hereafter referred to as *Zg*LamC$_{GH16\text{-}E142S}$. Like *Zg*LamC$_{GH16}$, a yield of 30 mg pure protein per litre of culture was obtained after two steps of chromatography (IMAC and SEC). The purification buffers were changed (HEPES instead of Tris–HCl for *Zg*LamC$_{GH16}$) to avoid protein precipitation during the concentration process (see §3.3). The hydrolysis of laminarin and of MLG by *Zg*LamC$_{GH16\text{-}E142S}$ was tested by the reducing-sugar assay, but no enzymatic activity was detected even after 24 h of hydrolysis, confirming the involvement of Glu142 in the catalytic machinery of *Zg*LamC$_{GH16}$.

3.2. *Zg*LamC$_{GH16}$ displays an endolytic mode of action

The hydrolysis of laminarin and MLG by *Zg*LamC$_{GH16}$ was monitored by FACE for 1 h and 30 min, respectively (Figs. 3*a*

and 3*b*). For both substrates, oligosaccharides with a relatively high degree of polymerization (DP) were initially released, progressively followed by oligosaccharides of smaller sizes. These product patterns indicate that *Zg*LamC$_{GH16}$ proceeds according to an endolytic mode of action. The degradation products of *Zg*LamC$_{GH16}$ were further analyzed. For laminarin, four standard β-1,3-glucan oligosaccharides (DP from 3 to 6) were digested by *Zg*LamC$_{GH16}$ to completion. The reducing end of the reaction products was labelled with ANTS and analyzed by FACE (Fig. 3*c*). Hydrolysis of the trisaccharide resulted in the release of two bands corresponding to a monosaccharide and a disaccharide. The released glucose was partially masked by the migration front of the fluorescent marker, but remained visible. The same degradation pattern was also observed for the other oligosaccharides (Fig. 3*c*). Thus, the smallest oligosaccharide that can be degraded by *Zg*LamC$_{GH16}$ is laminaritriose and the terminal products are glucose and laminaribiose. Finally, the degradation of a glucan tetrasaccharide containing two β-1,4 linkages separated by one β-1,3 linkage (G4G3G4G) was also monitored by FACE. ANTS labelling was undertaken either prior to or after the enzymatic reaction. When the tetrasaccharide was labelled first no cleavage was observed, indicating that the ANTS moiety hindered the action of *Zg*LamC$_{GH16}$. When labelling was undertaken after hydrolysis the reaction products migrate as two new bands corresponding to a monosaccharide and a trisaccharide (Fig. 3*d*). Therefore, as observed for *Zg*LamA$_{GH16}$ (Labourel *et al.*, 2014), *Zg*LamC$_{GH16}$ specifically cleaves β-1,4 linkages next to β-1,3 linkages, and the MLG trisaccharide and glucose are the terminal products.

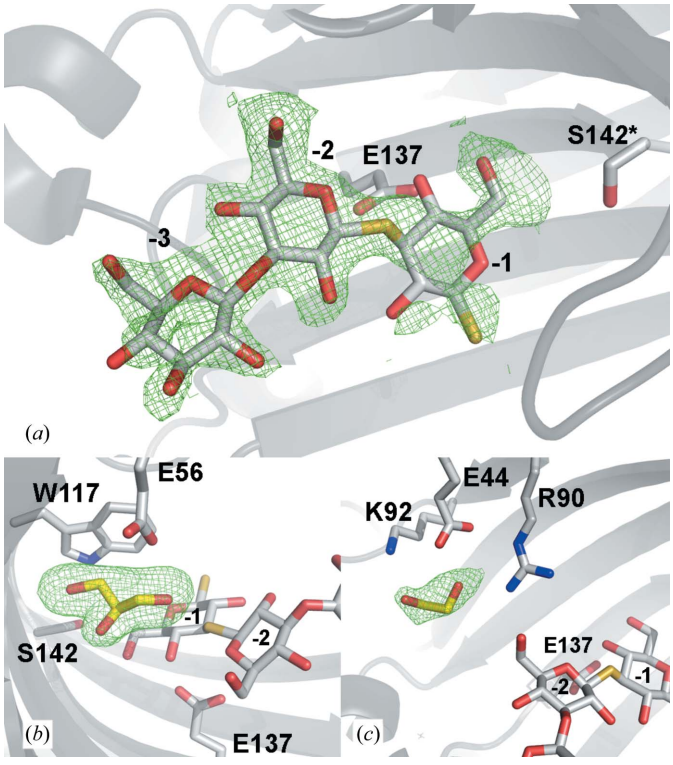

Figure 5
Electron-density map of the thio-β-1,3-glucan analogue and solvent ligands located in the active-site cleft of *Zg*LamC$_{GH16-E142S}$ molecule *B*. (*a*) OMIT map of the thio-oligosaccharide inhibitor spanning the subbinding sites −1 to 3. The electron density is contoured at the 2σ level. The best-fitting moiety of the oligosaccharide after refinement is overlaid on the electron density. (*b*) OMIT map (2.5σ level) showing the presence of a glycerol molecule adjacent to the −1 sugar-binding site. A tryptophan that stacks against this solvent molecule and Glu56 that forms a hydrogen bond to the solvent molecule are highlighted. (*c*) OMIT map (2.5σ level) showing the presence of an ethylene glycol molecule adjacent to the −2 sugar-binding site. The hydroxyl group at O6 of the glucose bound at subsite −2 points towards the pocket that contains the solvent molecule. The three residues Glu44, Arg90 and Lys92 interacting with this solvent molecule are highlighted.

3.3. Crystal structure of *Zg*LamC$_{GH16-E142S}$ ('apo form')

Prior to crystallization trials, *Zg*LamC$_{GH16}$ was submitted to a concentration step, but unfortunately the complete sample precipitated. Since we had already produced *Zg*LamC$_{GH16-E142S}$ in parallel, we decided to pursue the structural study using this mutated enzyme. Initially, we were not able to crystallize *Zg*LamC$_{GH16-E142S}$ alone. However, single crystals were obtained in the presence of purified laminaritetraoses produced by *Zg*LamA$_{GH16}$ (Labourel *et al.*, 2014). These crystals had good X-ray diffraction quality and the structure of *Zg*LamC$_{GH16-E142S}$ was solved at 1.5 Å resolution by molecular replacement using chain *A* of the laminarinase *Tm*LamCD from the hyperthermophilic bacterium *T. maritima* (47% sequence identity; PDB entry 3azx; Jeng *et al.*, 2011). The crystal is orthorhombic ($P2_12_12_1$) and two protein molecules are found in the asymmetric unit (from Asp24 to Lys254), as well as 426 water molecules. Surprisingly, there is no laminarin tetrasaccharide visible in the electron-density map, even though the presence of these oligosaccharides was essential in order to obtain crystals. The overall structure of *Zg*LamC$_{GH16-E142S}$ displays 13 β-strands and three small α-helices. The β-strands are organized into two twisted β-sheets typical of the jelly-roll fold of GH16 enzymes. *Zg*LamC$_{GH16-E142S}$ displays an open active-site cleft parallel to the inner β-sheet (Fig. 4*a*). The following ions and solvent ligands have been modelled into electron density: for protein chain *A* one Ca^{2+} ion, one Cl^- ion, one Mg^{2+} ion, two acetate ions and two ethylene glycols and for chain *B* one Ca^{2+} ion, two Cl^- ions, two Na^+ ions, one acetate ion and two ethylene glycols. In both chains the Ca^{2+} ion is found in the calcium-binding site conserved in most GH16-family enzymes (Michel *et al.*, 2001), with the exception of the xyloglucan endotransglycosylases (Johansson *et al.*, 2004) and xyloglucan hydrolases (Baumann *et al.*, 2007). Here, the calcium coordination displays identical pentagonal bipyramidal geometry in both chains. The base of the bipyramid is formed by bonds between the Ca^{2+} ion and Glu32 O, Asp247 O, Asp247 OD1 and two molecules of water. One tip of the bipyramid is provided by Gly70 O and the opposite tip is formed by a third water molecule. The water molecule at the bipyramid tip is further hydrogen-bonded to Glu32 OE1, while one of the water molecules of the base is hydrogen-bonded to Asp34 OD1. An acetate ion can be found in the catalytic cleft of chain *A* and is

hydrogen-bonded to three residues, Lys92, Glu44 and Arg90; in chain *B*, the nature of this molecule is less clear. Since no clear electron density for any oligosaccharide could be identified, this structure (PDB entry 4crq) can be considered as an 'apo' structure of *Zg*LamC$_{GH16\text{-}E142S}$.

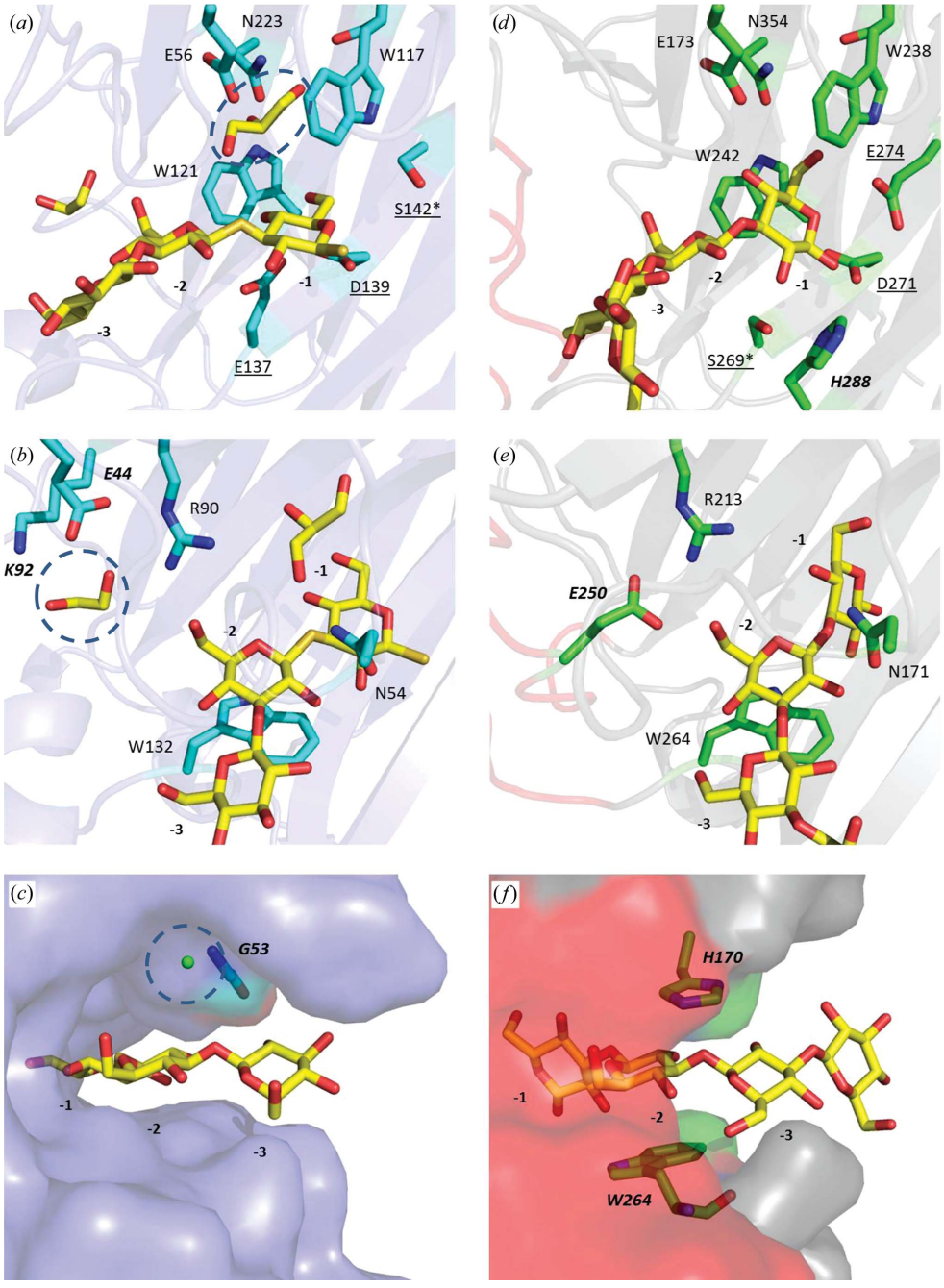

Figure 6
Molecular basis for the recognition of β-1,3-glucan by *Zg*LamC$_{GH16\text{-}E142S}$ and *Zg*LamA$_{GH16\text{-}E269S}$. (*a*), (*b*) and (*c*) correspond to *Zg*LamC$_{GH16\text{-}E142S}$ in complex with the thio-β-1,3-glucan analogue. Each panel focuses on a specific subsite (subsites −1, −2 and −3, respectively). In (*a*), (*b*) and (*c*) a dashed circle highlights the additional compounds found in the vicinity of the C6 hydroxyl group of each glucose moiety. A glycerol molecule is found in subsite −1 (*a*). An ethylene glycol molecule is found in subsite −2 (*b*). A chloride ion is found in subsite −3 (*c*). (*d*), (*e*) and (*f*) correspond to *Zg*LamA$_{GH16\text{-}E269S}$ in complex with a laminaritetraose (focusing on subsites −1, −2 and −3, respectively). The amino acids involved in substrate binding are displayed as sticks. The labels of the residues specific to each enzyme are shown in bold italics. The labels of the conserved catalytic amino acids of the GH16 family are underlined and an asterisk indicates each mutated catalytic residue. In (*c*) and (*f*) a transparent molecular surface is displayed to highlight the presence of an open cavity next to subsite −3 for *Zg*LamC$_{GH16\text{-}E142S}$ (*c*). ZgLamA$_{GH16\text{-}E269S}$ lacks such an open cavity (*f*).

3.4. Structure of *Zg*LamC$_{GH16\text{-}E142S}$ in complex with a thio-β-1,3-hexaglucan

In an additional attempt to obtain a complex structure, *Zg*LamC$_{GH16\text{-}E142S}$ was co-crystallized with a substrate analogue consisting of a β-1,3-glucan hexasaccharide displaying a benzyl group at the reducing end and in which the *O*-glycosidic bonds 3 and 4 were replaced by *S*-glycosidic linkages (Fig. 4*c*; Sylla, 2010). The X-ray structure was solved at 1.8 Å resolution (PDB entry 4cte) by molecular replacement using chain *A* of *Zg*LamC$_{GH16\text{-}E142S}$. The crystal is orthorhombic ($P2_12_12_1$) and two protein molecules (Asp24–Lys254) and 333 water molecules were found in the asymmetric unit. Each protein molecule also bound one Ca^{2+} ion, one Cl^- ion, an ethylene glycol and a glycerol, and one additional acetate ion was modelled in chain *B*. As in the 'apo' structure of *Zg*LamC$_{GH16\text{-}E142S}$, the Ca^{2+} ion was found in the binding site that is conserved in most GH16 enzymes, displaying a pentagonal bipyramidal geometry. In chain *B*, two of the base ligands (water molecules in chain *A*) were modelled as a bidentately binding acetate ion. Moreover, an oligosaccharide was clearly visible in the negative subsites of each protein (Fig. 5*a*). Additional electron density was also observed in the positive subsites, but was too disordered to be modelled as sugar units. In the more disordered chain *A*, only two glucose moieties were modelled spanning subsites −1 and −2. In chain *B*, three glucose moieties were modelled spanning subsites −1 to −3 (Fig. 5*a*). Superimposition of the 'apo' and

the complexed structures of ZgLamC$_{GH16\text{-}E142S}$ shows that no major conformational change occurs between the two structures. Since the substrate was visible in the electron-density map, it seems to have a higher affinity than the natural terminal products and was most likely to be bound to the protein with a *S*-glycosidic bond between the cleavage subsites −1 and +1. Taking into account this point and the structure of the glucan, an *S*-glycosidic bond was also modelled between subsites −1 and −2 (Fig. 5*a*). No significant positive or negative peak in the region of the *S*-glycosidic linkages was detected in the $F_o - F_c$ electron-density map (data not shown). In subsite −1 (Fig. 6*a*), the O4 hydroxyl group of the glucose residue is hydrogen-bonded to the nucleophile Glu137 OE2 (2.41 Å). Surprisingly, this glucose is found to be perpendicular to the two aromatic residues Trp117 and Trp121, which are conserved throughout the GH16 family (Michel *et al.*, 2001). Thus, the glucose ring of this analogue molecule does not adopt the parallel orientation at the cleavage subsite −1 that is usually observed in other structures of GH16 complexes. Moreover, density corresponding to a glycerol was found in a pocket above the −1 subsite in both chains (Fig. 5*b*). These glycerol molecules make hydrogen bonds to three residues (Fig. 6*a*). O3 is bound to Glu56 OE2 (2.84 Å) and water molecule HOH2038 (2.36 Å; distances are given for molecule *B*). O2 makes a hydrogen bond to Asn223 OD1 (2.64 Å), while O1 makes a hydrogen bond to Asn223 ND2 (2.78 Å) and the carbonyl of Trp117 (2.81 Å). Trp117 also interacts through hydrophobic stacking with the carbon backbone of the glycerol. At subsite −2 (Fig. 6*b*), the glucose unit makes hydrogen bonds to Asn54 OD1 and Arg90 NH2, and Trp132 serves as a hydrophobic platform. In both chains, an ethylene glycol is also found in a pocket located next to subsite −2 (Fig. 5*c*), and is hydrogen-bonded to Lys92 NZ, Glu44 OE2 and Arg90 NH2. Subsite −3 of ZgLamC$_{GH16\text{-}E142S}$ is characterized by a hydrogen bond between O2 and Gly53 O (2.46 Å; Fig. 6*c*). The O6 is solvent-exposed and above this subsite a Cl^- ion is found to be associated with two molecules of water (HOH2193 and HOH2035). The Cl^- ion is close to the hydrophobic surface made up by the lateral and the main chain of Trp52. It also interacts with Tyr49 N. HOH2193 makes a hydrogen bond to O5 (3.07 Å) and O6 (3.35 Å) of the glucose unit in subsite −3. Strikingly, the O6 groups of the glucose moieties in subsites −1, −2 and −3 point towards pockets containing a glycerol, an ethylene glycol and a chloride ion, respectively. A conserved structural water molecule (HOH2030 in chain *A* and HOH2038 in chain *B*) was found to make hydrogen bonds to O5 (2.77 Å) and O6 (2.82 Å) of the glucose unit at subsite −2 and to Arg90 NH1 (2.87 Å) and Trp52 O (2.75 Å).

3.5. Comparison of the ZgLamC$_{GH16\text{-}E142S}$–thioglucan and ZgLamA$_{GH16\text{-}E269S}$–laminaritetraose complex structures

The laminarinases ZgLamA$_{GH16}$ and ZgLamC$_{GH16}$ are relatively divergent in sequence (37% identity; Fig. 1*b*), but superimposition of the ZgLamA$_{GH16\text{-}E269S}$–laminaritetraose (Labourel *et al.*, 2014) and ZgLamC$_{GH16\text{-}E142S}$–inhibitor complexes results in a low root-mean-square deviation (0.91 Å over 199 matched C^α atoms). Both complex structures display sugar molecules bound to the negative subsites −1, −2 and −3 (except where mentioned, all of the amino acids are numbered as in ZgLamC$_{GH16\text{-}E142S}$). At subsite −1 the glucose unit does not adopt the same position in the two structures (Figs. 6*a* and 6*d*). In ZgLamA$_{GH16\text{-}E269S}$ the glucose is typically found parallel to the two conserved tryptophans (Trp117 and Trp121), while this sugar binds perpendicularly to these aromatic residues in ZgLamC$_{GH16\text{-}E142S}$. The glucose moiety establishes more hydrogen bonds with ZgLamA$_{GH16\text{-}E269S}$, with O6 interacting with Trp238 NE1 and O1 with His288 (ZgLamA$_{GH16\text{-}E269S}$ numbering), a histidine that is conserved throughout the GH-B clan (Michel *et al.*, 2001). The pocket located above subsite −1 is also found in ZgLamA$_{GH16\text{-}E269S}$ and all residues forming this pocket are conserved (Asn223, Tyr60, Glu56 and Trp117). The glucose units in subsites −2 and −3 can be partially superimposed and they adopt a similar orientation in both enzymes. Three amino acids are conserved between subsites −2 (Figs. 6*b* and 6*e*): Arg90, Asn54 and Trp132. In ZgLamA$_{GH16\text{-}E269S}$ a fourth residue participates in subsite −2, Glu250, which belongs to the additional loop of this enzyme and makes a hydrogen bond to the glucose unit. This glutamate is absent in ZgLamC$_{GH16\text{-}E142S}$, which instead displays a pocket next to subsite −2 which is occupied by an ethylene glycol molecule. In ZgLamC$_{GH16\text{-}E142S}$ subsite −3 consists of a hydrogen bond between O2 of the glucose unit and the carbonyl of Gly53, while in ZgLamA$_{GH16\text{-}E269S}$ the carbonyl of Trp264 is hydrogen-bonded to the O6 hydroxyl group of the glucose (Figs. 6*c* and 6*f*; Labourel *et al.*, 2014).

4. Discussion

Brown algae produce a variety of β-1,3-glucans with different biological functions: the M-series and G-series of branched laminarins (Read *et al.*, 1996), linear insoluble laminarins (Nelson & Lewis, 1974; Rioux *et al.*, 2010) and even semi-crystalline callose in the sieve tubes of kelps (Laminariales; Parker & Huber, 1965). To face this physicochemical diversity, the seaweed-associated bacterium *Z. galactanivorans* possesses a multi-enzymatic system of five putative β-1,3-glucanases (four GH16s, ZgLamA–ZgLamD, and one GH64, ZgLamE) with different modular architectures. The four GH16 modules are quite divergent, with sequence identity ranging from 29 to 37%. Moreover, these β-glucanases are predicted to have different cellular localizations. For instance, ZgLamA is predicted to be a lipoprotein located in the outer membrane (Labourel *et al.*, 2014), while ZgLamC features an N-terminal signal peptide and a C-terminal Por secretion system (PorSS) domain. Such conserved C-terminal domains are also present in two enzymes from *Z. galactanivorans* already known to be secreted into the extracellular medium: the κ-carrageenase ZgCgkA (Barbeyron *et al.*, 1998) and the β-agarase ZgAgaA (Jam *et al.*, 2005). Therefore, ZgLamC is likely to be targeted to the periplasm by the Sec system and then exported across the outer membrane by PorSS (Sato *et al.*, 2010). Altogether, the sequence divergences and the

differences in modular architecture and potential localizations suggest that the β-glucanases of *Z. galactanivorans* have distinct and/or complementary roles. Recently, we have characterized the first enzyme of this laminarolytic system, *Zg*LamA$_{GH16}$. This enzyme is highly efficient and almost exclusively active on algal laminarin. The structure of *Zg*LamA$_{GH16}$ in complex with laminaritetraose has revealed a unique topology within the GH16 family (a bent active site; Fig. 4*b*), which explains this exquisite adaptation to algal laminarin (Labourel *et al.*, 2014).

In the present work, we have undertaken a first comparative analysis to test the hypothesis of the differing or complementary functions of the β-glucanases of *Z. galactanivorans*. Thus, we have overexpressed and purified the GH16 catalytic module of *Zg*LamC. The recombinant enzyme *Zg*LamC$_{GH16}$ is active on both laminarin and MLG, with a catalytic efficiency (k_{cat}/K_m) three times higher for laminarin than for MLG. This enzyme acts according to an endolytic mode of action (Figs. 3*a* and 3*b*). Its minimal substrate is laminaritriose, releasing glucose and laminaribiose (Fig. 3*c*). *Zg*LamC$_{GH16}$ also cleaves β-1,4-linkages next to β-1,3-linkages in MLG, giving the terminal products glucose and the trisaccharide G4G3G (Fig. 3*d*). Interestingly, *Zg*LamC$_{GH16}$ is less efficient on linear laminarin than *Zg*LamA$_{GH16}$ (Labourel *et al.*, 2014; k_{cat}/K_m of 59 213 and 82 000 M^{-1} s^{-1}, respectively), but approximately six times more active on MLG (k_{cat}/K_m of 21 662 and 3678 M^{-1} s^{-1}, respectively). These differences in catalytic efficiency can be explained by the respective active-site topologies of *Zg*LamC$_{GH16}$ and *Zg*LamA$_{GH16}$. Indeed, the straight-cleft topology of *Zg*LamC$_{GH16}$ (Fig. 4*a*) is a good compromise to provide significant activity on both MLG (straight shape) and laminarin (helical shape), while the bent active site of *Zg*LamA$_{GH16}$ (Fig. 4*b*) is optimized for laminarin recognition but results in a much weaker activity on MLG (Labourel *et al.*, 2014).

The lower affinity for linear β-1,3-glucan in comparison to *Zg*LamA$_{GH16}$ was also highlighted by our difficulty in obtaining a complex structure of *Zg*LamC$_{GH16\text{-}E142S}$ with native oligo-laminarins. Eventually, we succeeded in obtaining a complex structure in the presence of a thio-β-1,3-glucan analogue (Figs. 5*a* and 6). *Zg*LamC$_{GH16\text{-}E142S}$ and *Zg*LamA$_{GH16\text{-}E269S}$ both display three negative subsites, but *Zg*LamC$_{GH16\text{-}E142S}$ establishes fewer interactions with the oligosaccharide in subsites -2 and -3, which could contribute to its weaker efficiency on linear β-1,3-glucan. However, the most striking feature of this complex structure is the presence of unexpected compounds in the vicinity of the OH6 hydroxyl group of each glucose unit; Figs. 5*b* and 5*c*). The glycerol molecule in subsite -1 could be responsible for the unusual position of the glucose residue, which is perpendicular to Trp121 (Fig. 6*a*). This perpendicular position is probably a crystallization artifact, possibly owing to the presence of the adjacent glycerol molecule and the thioglycosidic linkages in the analogue substrate. Indeed, subsites -1 of both laminarinases are identical and in *Zg*LamA$_{GH16\text{-}E269S}$ the glucose residue is stacked against the conserved tryptophan Trp242 (Fig. 6*d*), as typically observed in the GH16 family. In contrast, the presence of an ethylene glycol next to subsite -2 is likely to have biological significance. This compound is located in a pocket unique to *Zg*LamC$_{GH16\text{-}E142S}$ and is hydrogen-bonded to Glu44, Arg90 and Lys92 (Fig. 6*b*). Interestingly, Glu44 and Lys92 are conserved in the sequences of the closest homologues of *Zg*LamC$_{GH16}$ (data not shown). This cavity does not exist in *Zg*LamA$_{GH16\text{-}E269S}$ and is spatially replaced by Glu250, which belongs to the additional loop typical of this laminarinase (Figs. 1*b* and 6*e*). This pocket is ideally located to receive a β-1,6-glucose side chain, and the binding of an ethylene glycol in the *Zg*LamC$_{GH16\text{-}E142S}$–thioglucan complex structure strengthens this hypothesis. Similarly, the OH6 hydroxyl group of glucose in subsite -3 is oriented towards a large open cavity which contains a chloride ion (Fig. 6*c*). Thus, there is no hindrance to the presence of a β-1,6-glucose branch. In *Zg*LamA$_{GH16\text{-}E269S}$ there is no equivalent space owing to the presence of the additional loop, and the OH6 hydroxyl group of the glucose in subsite -3 is already involved in a hydrogen bond to the carbonyl group of Trp264 (Fig. 6*f*). Thus, *Zg*LamC$_{GH16}$ features unique cavities in the active site which render the specific binding of branched laminarin plausible.

Altogether, these results confirm our initial assumption about the functional diversity of the β-glucanases from *Z. galactanivorans*, with at least two type of enzymes. While *Zg*LamA is essentially specialized for linear laminarin (Labourel *et al.*, 2014), *Zg*LamC$_{GH16}$ has a more balanced efficiency for the degradation of laminarin and MLG. Moreover, the presence of additional pockets in the active cleft of *Zg*LamC$_{GH16}$ suggests that this enzyme is well adapted for the degradation of branched motifs in laminarin chains. The significant activity of *Zg*LamC$_{GH16}$ on MLG could also have an ecological relevance. Although MLG is not yet known to be a component of brown algal cell walls (Popper *et al.*, 2011), sulfated MLGs have been identified in some species of red seaweeds (Lechat *et al.*, 2000) and could also be a potential substrate of *Zg*LamC.

This work was supported by the French National Research Agency with regard to the investment expenditure program IDEALG (http://www.idealg.ueb.eu/, grant agreement No. ANR-10-BTBR-04). The PhD fellowship of AL was funded by the French Ministry of Higher Education and Research. BS thanks the Région Bretagne for a fellowship. The authors are grateful for financial support from the Cancéropole Grand Ouest (Axis Produits de la Mer en Cancérologie and MabImpact Network). We are indebted to local contacts for their support during data collection at beamlines PROXIMA1, SOLEIL, Saint Aubin, France and BM14, ESRF, Grenoble, France.

References

Barbeyron, T., Gerard, A., Potin, P., Henrissat, B. & Kloareg, B. (1998). *Mol. Biol. Evol.* **15**, 528–537.

Barbeyron, T., L'Haridon, S., Corre, E., Kloareg, B. & Potin, P. (2001). *Int. J. Syst. Evol. Microbiol.* **51**, 985–997.

Baumann, M. J., Eklöf, J. M., Michel, G., Kallas, A. M., Teeri, T. T., Czjzek, M. & Brumer, H. (2007). *Plant Cell*, **19**, 1947–1963.

Bleicher, L., Prates, E. T., Gomes, T. C., Silveira, R. L., Nascimento, A. S., Rojas, A. L., Golubev, A., Martínez, L., Skaf, M. S. & Polikarpov, I. (2011). *J. Phys. Chem. B*, **115**, 7940–7949.

Duarte, C. M., Middelburg, J. J. & Caraco, N. (2005). *Biogeosciences*, **2**, 1–8.

Emsley, P., Lohkamp, B., Scott, W. G. & Cowtan, K. (2010). *Acta Cryst.* D**66**, 486–501.

Evans, P. (2006). *Acta Cryst.* D**62**, 72–82.

Gouet, P., Robert, X. & Courcelle, E. (2003). *Nucleic Acids Res.* **31**, 3320–3323.

Groisillier, A., Hervé, C., Jeudy, A., Rebuffet, E., Pluchon, P. F., Chevolot, Y., Flament, D., Geslin, C., Morgado, I. M., Power, D., Branno, M., Moreau, H., Michel, G., Boyen, C. & Czjzek, M. (2010). *Microb. Cell Fact.* **9**, 45.

Groisillier, A., Shao, Z., Michel, G., Goulitquer, S., Bonin, P., Krahulec, S., Nidetzky, B., Duan, D., Boyen, C. & Tonon, T. (2014). *J. Exp. Bot.* **65**, 559–570.

Hehemann, J. H., Correc, G., Barbeyron, T., Helbert, W., Czjzek, M. & Michel, G. (2010). *Nature (London)*, **464**, 908–912.

Jackson, P. (1990). *Biochem. J.* **270**, 705–713.

Jam, M., Flament, D., Allouch, J., Potin, P., Thion, L., Kloareg, B., Czjzek, M., Helbert, W., Michel, G. & Barbeyron, T. (2005). *Biochem. J.* **385**, 703–713.

Jeng, W.-Y., Wang, N.-C., Lin, C.-T., Shyur, L.-F. & Wang, A. H.-J. (2011). *J. Biol. Chem.* **286**, 45030–45040.

Johansson, P., Brumer, H., Baumann, M. J., Kallas, A. M., Henriksson, H., Denman, S. E., Teeri, T. T. & Jones, T. A. (2004). *Plant Cell*, **16**, 874–886.

Juncosa, M., Pons, J., Dot, T., Querol, E. & Planas, A. (1994). *J. Biol. Chem.* **269**, 14530–14535.

Karlsson, E. N., Hachem, M. A., Ramchuran, S., Costa, H., Holst, O., Svenningsen, Å. F. & Hreggvidsson, G. O. (2004). *FEMS Microbiol. Lett.* **241**, 233–242.

Keitel, T., Simon, O., Borriss, R. & Heinemann, U. (1993). *Proc. Natl Acad. Sci. USA*, **90**, 5287–5291.

Kidby, D. K. & Davidson, D. J. (1973). *Anal. Biochem.* **55**, 321–325.

Krah, M., Misselwitz, R., Politz, O., Thomsen, K. K., Welfle, H. & Borriss, R. (1998). *Eur. J. Biochem.* **257**, 101–111.

Labourel, A., Jam, M., Jeudy, A., Hehemann, J. H., Czjzek, M. & Michel, G. (2014). *J. Biol. Chem.* **289**, 2027–2042.

Lechat, H., Amat, M., Mazoyer, J., Buléon, A. & Lahaye, M. (2000). *J. Phycol.* **36**, 891–902.

Leslie, A. G. W. (2006). *Acta Cryst.* D**62**, 48–57.

Lombard, V., Golaconda Ramulu, H., Drula, E., Coutinho, P. M. & Henrissat, B. (2014). *Nucleic Acids Res.* **42**, D490–D495.

Martin, M., Portetelle, D., Michel, G. & Vandenbol, M. (2014). *Appl. Microbiol. Biotechnol.* **98**, 2917–2935.

McBride, M. J. & Zhu, Y. (2013). *J. Bacteriol.* **195**, 270–278.

Michel, G., Chantalat, L., Duee, E., Barbeyron, T., Henrissat, B., Kloareg, B. & Dideberg, O. (2001). *Structure*, **9**, 513–525.

Michel, G. & Czjzek, M. (2013). *Marine Enzymes for Biocatalysis. Sources, Biocatalytic Characteristics and Bioprocesses of Marine Enzymes*, edited by A. Trincone, pp. 429–464. Cambridge: Woodhead Publishing. doi:10.1533/9781908818355.3.429.

Michel, G., Tonon, T., Scornet, D., Cock, J. M. & Kloareg, B. (2010*a*). *New Phytol.* **188**, 67–81.

Michel, G., Tonon, T., Scornet, D., Cock, J. M. & Kloareg, B. (2010*b*). *New Phytol.* **188**, 82–97.

Nelson, T. E. & Lewis, B. A. (1974). *Carbohydr. Res.* **33**, 63–74.

O'Sullivan, L., Murphy, B., McLoughlin, P., Duggan, P., Lawlor, P. G., Hughes, H. & Gardiner, G. E. (2010). *Mar. Drugs*, **8**, 2038–2064.

Parker, B. C. & Huber, J. (1965). *J. Phycol.* **1**, 172–179.

Percival, E. G. V. & Ross, A. G. (1951). *J. Chem. Soc.*, pp. 720–726.

Popper, Z. A., Michel, G., Hervé, C., Domozych, D. S., Willats, W. G., Tuohy, M. G., Kloareg, B. & Stengel, D. B. (2011). *Annu. Rev. Plant Biol.* **62**, 567–590.

Read, S. M., Currie, G. & Bacic, A. (1996). *Carbohydr. Res.* **281**, 187–201.

Rioux, L. E., Turgeon, S. L. & Beaulieu, M. (2010). *Phytochemistry*, **71**, 1586–1595.

Roberts, S. M. & Davies, G. J. (2012). *Methods Enzymol.* **510**, 141–168.

Rousvoal, S., Groisillier, A., Dittami, S. M., Michel, G., Boyen, C. & Tonon, T. (2011). *Planta*, **233**, 261–273.

Sato, K., Naito, M., Yukitake, H., Hirakawa, H., Shoji, M., McBride, M. J., Rhodes, R. G. & Nakayama, K. (2010). *Proc. Natl Acad. Sci. USA*, **107**, 276–281.

Stone, B. A. (2009). *Chemistry, Biochemistry and Biology of (1→3)-β-Glucans and Related Polysaccharides*, edited by A. Bacic, G. B. Fincher & B. A. Stone, pp. 5–46. New York: Academic Press.

Studier, F. W. (2005). *Protein Expr. Purif.* **41**, 207–234.

Sylla, B. (2010). PhD thesis. Université de Rennes 1, France.

Thomas, F., Barbeyron, T., Tonon, T., Génicot, S., Czjzek, M. & Michel, G. (2012). *Environ. Microbiol.* **14**, 2379–2394.

Thomas, F., Lundqvist, L. C., Jam, M., Jeudy, A., Barbeyron, T., Sandstrom, C., Michel, G. & Czjzek, M. (2013). *J. Biol. Chem.* **288**, 23021–23037.

Vagin, A. A., Steiner, R. A., Lebedev, A. A., Potterton, L., McNicholas, S., Long, F. & Murshudov, G. N. (2004). *Acta Cryst.* D**60**, 2184–2195.

Vagin, A. & Teplyakov, A. (2010). *Acta Cryst.* D**66**, 22–25.